Terahertz Quantum Cascade Lasers - first demonstration and novel concepts

Alessandro Tredicucci†, Rüdeger Köhler†, Lukas Mahler†, Harvey E Beere‡, Edmund H Linfield‡ and David A Ritchie‡

† NEST-INFM and Scuola Normale Superiore, Piazza dei Cavalieri 7, 56126 Pisa, Italy

‡ Cavendish Laboratory, University of Cambridge, Madingley Road, Cambridge CB3 0HE, United kingdom

Abstract. Quantum cascade (QC) lasers operating at terahertz frequencies were demonstrated two years ago, and, since then, their development has proceeded at a very rapid pace. The gain medium of the first devices was based on chirped superlattices, and a resonator relying on the surface-plasmon concept was employed to achieve a large optical confinement with concomitant low propagation losses. Laser action was achieved at 4.4 THz, in pulsed mode and at temperatures up to 50 K. Improved fabrication allowed continuous-wave (cw) operation and increased the operating temperature to 75 K. Using a similar active region, lasing at 3.5 THz was achieved. More recently, various groups have introduced several new design concepts such as bound-to-continuum transitions and extraction of carriers via resonant phonon scattering, leading to pulsed operation up to 140 K, output powers of up to 50 mW, and cw operation up to 93 K. The lowest emission frequency is now 2.1 THz, tackling the technologically important region of 1.5 - 2.5 THz. Stable single-mode emission under all operating conditions has also recently become a reality thanks to the adoption of distributed feedback resonators. This rapid and substantial progress underlines the growing potential of QC lasers in THz photonics.

E-mail: a.tredicucci@sns.it

1. Introduction

Semiconductor devices traditonally account for a large share of the sources of electromagnetic waves, emitting frequencies from kHz up to those of ultaviolet light. The terahertz range, however, has remained for long substantially uncovered. Transport-based devices are widely available at GHz frequencies and up, but their operation above 1 THz faces major physical obstacles. On the other hand, transition-based photonic systems such as diode lasers are utilized down to about 12 THz; their operation at longer wavelengths is hindered by difficulties of both fundamental and technological nature.
Quantum Cascade Lasers (QCLs) [1] are unipolar semiconductor lasers that are based on intersubband transitions in a specifically engineered heterostructure. Contrary to conventional laser diodes, where the optical transition takes place across the band gap (interband), thus leading to the recombination of electrons with holes, in these novel devices only electrons are involved and the transition occurs between subbands belonging to the conduction band (intersubband). The energy and envelope functions of the subbands can be controlled by the thickness of the individual layers, quantum wells and barriers, and by the applied bias. Therefore, the band gap of the choice materials is in first instance irrelevant to the energy of the emitted photons and hence technologically mature systems like InGaAs/AlInAs or GaAs/AlGaAs can be used in a wide range of emission wavelengths. Population inversion between two specific subbands is achieved via the engineering of tunneling rates and electron-phonon scattering matrix elements. The active regions hosting the optical transition are connected by injector/collector regions. These are superlattice structures whose states resemble a miniband that collects electrons from the upstream active region, cools down the carrier distribution and injects them again into the upper laser level of the following active region. Injector/collector regions and active regions form a building block (so-called period) that can be repeated many times (typically 25 - 100). Under appropriate bias, all periods line up to form the potential 'cascade', the active core of the laser, which the electrons travel downstream, emitting ideally one photon at each step of the cascade. Quantum cascade lasers have been first operated in the mid-infrared [1], and the range of emission wavelengths has increased widely ever since, with concomitant tremendous improvements in their performance, eventually leading to continuous-wave operation at room-temperature [2, 3]. However, the phonon reststrahlen band (located at 8-9 THz in the commonly employed systems) was considered to be an insuperable barrier in the further expansion to lower emission frequencies. In fact, while electroluminescence at THz frequencies was observed by several groups [4, 5, 6], none of these structures exhibited population inversion. This can be understood also from the difficulty of gaining sufficient control of scattering rates at such low energies, since an extension of the phonon-scattering based approach is not straightforward. Another challenge was the development of a suitable waveguide to confine light of such long wavelength to an epilayer compatible with molecular beam epitaxy (MBE) technology without imposing high absorption losses onto the laser mode. Lasing was first reported two years ago [7], and since then improved fabrication has led

to continuous-wave operation and high output powers [8, 9, 10]. Thanks to the introduction of new design concepts, lasers operating at ever longer wavelengths and higher temperatures are being realized and the first practical applications are being developed [11, 12, 13, 14, 15, 16]. Here, we analyse the fundamentals of THz QC lasers, discuss recent performance improvements, and present our latest progress concerning single mode operation and frequency extension.

2. Principle and first realization

Figure 1 (a) shows a portion of the conduction band structure of the first THz QC laser. The moduli squared of the relevant wavefunctions are displayed, with the laser transition taking place between the two levels drawn in boldface. This active region follows the concept of chirped superlattices (SL) [17], which represent an elegant solution to achieve population inversion when precise tailoring of the lifetimes is too complex. Montecarlo simulations [18] and electroluminescence measurements [19] immediately showed how promising this approach was towards providing gain at THz frequencies. The SL period and duty-cycle are varied in order to realize a flat-band condition under applied bias, and the optical transition takes place between the first and second miniband rather than between individual electronic levels. The main characteristics of this structure are the large dipole matrix element of 7.8 nm at an emission energy of 18 meV (4.3 THz) and the wide injector miniband, highlighted by the shaded area in Fig. 1. The lower laser level 1 is strongly coupled to this miniband which, in conjunction with the large miniband dispersion of 17 meV, facilitates the achievement of population inversion. The strong coupling leads to a rapid extraction of carriers from state 1 owing to the large scattering matrix elements between this level and the injector states [18]. Moreover, it reduces the non-radiative scattering rate τ_{21}^{-1} from the upper laser level 2 directly into 1, as electrons in the first can scatter to a whole dense miniband of states. Finally, the large dispersion of the miniband supports a wide range of currents and voltages in the operating characteristics, which is necessary for the achievement of high output powers, and, additionally, suppresses thermal backfilling from the downstream active region.

On the other side, efficient waveguiding of THz radiation inside a semiconductor heterostructure represents another challenge, owing to the long wavelength, typically resulting in small confinement factors, and to the high losses caused by free-carrier absorption. Conventionally, long-wavelength (up to $\lambda \sim 24\mu$m) QC lasers [20, 21] made use of a waveguide concept introduced by Sirtori *et al.* [22], that relies on surface-plasmons [23]. In the direction perpendicular to the interface, the optical mode peaks at the interface and decays exponentially to both sides, with the decay constants controlled by the wavelength of the light and by the dielectric constant of the materials at each side of the interface. At THz wavelengths and in the GaAs/AlGaAs system, however, such a single-plasmon waveguide would lead to very small confinement factors.

In our laser the waveguide relies on the presence of a thin, highly-doped layer which

was grown directly underneath the low-doped stack of active SLs. Its negative dielectric constant, comparable in modulus to the one of active stack and substrate, and its small thickness merge the two surface plasmons existing at the two interfaces into a single mode, whose penetration into the surrounding semiconductor is at the same time minimized, resulting in a very tight confinement and low optical losses. The calculated mode profile of the actual waveguide adopted in the first devices is shown in Fig. 1 (b); we calculate a confinement factor of $\Gamma = 0.47$ and optical losses of $\alpha_w = 12$ cm^{-1} [7].
This structure was grown by molecular beam epitaxy on a semi-insulating GaAs substrate, starting with the 800 nm thick n-doped (2×10^{18}cm^{-3}) GaAs layer, followed by 104 repetitions of the superlattice (thicknesses are given in the caption of Fig. 1), and terminated by a 200 nm thick n-doped (5×10^{18}cm^{-3}) GaAs layer to facilitate electrical contacting. The fabrication of the laser in ridges is typically performed with optical contact lithography, and from the first demonstration has gone through some optimization, mostly concerning contact geometry and composition, as described in detail in Ref. [10]. Facets of the cleaved laser bars are left either untreated or a high-reflection coating can be deposited on the back facet. For the measurements in our set-up, the laser bars are soldered onto a copper block using an In-Ag alloy, wire-bonded and mounted onto the cold-finger of a continuous-flow cryostat equipped with polyethylene windows. Light is collected using an f/1 off-axis parabolic mirror, sent through an FTIR-spectrometer and detected with a DTGS (deuterated triglycine sulphate) detector or a He-cooled Si bolometer. Light-current (L-I) characteristics in continuous wave (cw) operation are recorded by mounting a Winston cone in front of the laser facet and using a calibrated pyroelectric radiometer.
Figure 2 shows exemplary light-current characteristics of a device from a sample nominally identical to the first one. Data have been recorded in pulsed operation at different heat sink temperatures. At 5 K the maximum output power is around 3 mW, with threshold current densities as low as 130 Acm^{-2}. This particular laser shows the best thermal performance with a highest operating temperature of 75 K. Back-facet coated lasers result in larger emitted powers with improved cw capability. More than 4 mW per facet (in a set-up with an estimated 33% collection efficiency) have been achieved in cw, with a maximum temperature of 48 K [10].

3. High-temperature and long-wavelength operation

A THz QC laser that operates above liquid nitrogen, at temperatures up to 95 K, was first demonstrated by Scalari *et al.* [12]. It is based on a so-called bound-to-continuum (BTC) design [24], in which the SL concept is re-interpreted making use of a spatially diagonal transition to reduce the non-radiative loss of carriers from the upper laser level. This approach, though already quite successful, addresses only the upper state lifetime τ_2, while it is also very important to reduce the lifetime τ_1 of the lower lasing state 1. In the BTC design as well as in the previously-described chirped SL laser, extraction of carriers from level 1 mainly occurs through electron-electron-activated scattering into

states of the injector miniband. Efficient depletion of the lower state in these THz QC lasers is hindered by the insufficient cooling of the electron distribution, and the 'effective' lifetime τ_1, defined as in the inverse of the *net* scattering rate out of level 1, is strongly influenced by the electronic temperature due to the small dispersion of the injector miniband. In mid-infrared QC lasers, on the contrary, population inversion up to room-temperature and above is maintained by exploiting resonant fast electron-phonon scattering as the extraction process. A similar concept was recently introduced by Williams *et al.* [25] in THz QC lasers. Albeit promising, the first implementation exhibited quite high threshold current densities of 800 Acm^{-2}, that could be attributed to the poor control of electrical transport in such virtually injector-less structures. More recent developments have partially improved this issue and, also thanks to the use of fully metallic waveguides with nearly unity confinement factor, record high operating temperatures of 140 K (93 K in cw) have been achieved, at the expense however of a low output power [15, 26].

Here, we describe an alternative design based on interlacing photon and phonon emitting stages bridged by appropriate minibands [27]. Figure 3 shows a portion of the conduction band structure under an applied bias of 5.4 kV/cm. The wavelength in this case is 80μm. While the minibands, labeled A and B in Fig. 3, ensure good control of the transport characteristics, and allow for a wide range of currents and voltages, the LO phonon stage efficiently shortens the effective lifetime τ_1 of the lower lasing state. Extraction of carriers from level 1 still occurs through e-e scattering into the states comprising miniband A, but the lower states of the miniband are strongly coupled to the phonon stage, and therefore rapid extraction from these states is provided by e-p scattering. For a more detailed description of the band structure, waveguide and device processing we refer to Ref. [27]. The expectation of a short lifetime τ_1 and negligible thermal backfilling is indeed confirmed in this structure, as is best seen from the L-I characteristics in Fig. 3. The slope efficiency, i.e., the derivative of the output power vs. injection current is virtually independent on temperature, which indicates a constant τ_1. In fact, lasing at temperatures higher than the currently achieved 95 K appears to be limited solely by the maximum current density that can be passed through the device. The residual threshold dependence on temperature is then mainly determined by the non-radiative relaxation of upper state electrons, which could be reduced in structures with a more diagonal optical transition.

Several applications particularly in astronomy and chemical sensing involve detection at frequencies in the range 1.5 to 2.5 THz. A chirped superlattice design similar to the one of section 2 led to lasing at 3.5 THz with comparable performance [11]. Moving towards longer wavelengths, however, the BTC concept appears to be more favorable and forms the basis of lasers emitting at 2.9 THz [13, 28] and 2.3 THz [29]. The diagonal character (in real space) of the optical transition facilitates a selective carrier injection, particularly at low transition energies. We have realized BTC lasers for specific sensing applications, emitting at frequencies from 4.8 THz down to 2.4 THz. In Fig. 4 we show the emission spectra of two such lasers, together with the cw L-I characteristics of a

2.5 THz QC laser. The latter shows a record low threshold current density of about 75 A/cm^2 with a high cw output power of 6 mW per facet (33% collection efficiency) and a maximum cw operating temperature of 56 K. These devices are all based on the waveguide concept employed for the first 4.4 THz QC laser [7]; fully metallic waveguides possess a near unity confinement factor [14] and could be better suited for even longer wavelengths as witnessed by the recent realization of a 2.1 THz laser [30].
The implementation of THz QC lasers in spectroscopic applications as direct sources or local oscillators requires stable, repeatable single-mode emission. We have recently succeeded in fabricating a distributed feedback (DFB) resonator by inserting a special grating into the waveguide of a THz QC lasers [31]. A complex-coupling scheme based on a combination of wet chemical etching into the topmost layer of the heterostructure with selectively annealed ohmic contacts leads to stable, predictable single-mode emission with side-mode suppression ratios of better than 20 dB. Fig. 5 shows the output spectra at 4.34 THz and 4.43 THz obtained by using grating periods of 9.4 and 9.2 μm, respectively, in a structure nominally identical to Ref. [7]. The multi-mode spectra resulting with a purely-index coupled grating are also displayed for comparison. The output power of these QC-DFB devices is about 2 mW at low temperatures, showing that device performance is not substantially affected by the presence of the gratings.

4. Summary and outlook

Since their initial demonstration THz QC lasers have made rapid and substantial progress. Improved device fabrication and novel concepts such as phonon-assisted structures have allowed cw operation and raised the maximum pulsed operating temperature to 140 K, feeding the hope that THz QC lasers could be operated on Peltier-cooled stages. Output power levels have also seen an increase by at least an order of magnitude. Available emission frequencies now range from 2.1 THz up to 4.8 THz and single-mode DFB devices have been fabricated. Though many issues (tunability, lower emission frequencies, room temperature) still remain open and are being widely investigated with a variety of approaches, the above-described developments underline the high potential of QC lasers in the emerging field of THz photonics.

Acknowledgments

This work was supported in part by Physical Sciences Inc. of Andover and by the Fondazione Cassa di Risparmio di Pisa

References

[1] Faist J, Capasso F, Sivco D L, Sirtori C, Hutchinson A H and Cho A Y 1994 *Science* **264** 553
[2] Beck M, Hofstetter D, Aellen T, Faist J, Osterle U, Ilegems M, Gini E and Melchior H 2002 *Science* **295** 301
[3] Evans A, Yu J S, David J, Doris L, Mi K, Slivken S and Razeghi M 2004 *Appl. Phys. Lett.* **84** 314

[4] Rochat M, Faist J, Beck M, Oesterle U and Ilegems M 1998 *Appl. Phys. Lett.* **73** 3724
[5] Williams B S, Xu B, Hu Q and Melloch M R, 1999 *Appl. Phys. Lett.* **75** 2927
[6] Ulrich J, Zobl R, Schrenk W, Strasser G, Unterrainer K and Gornik E 2000 *Appl. Phys. Lett.* **77** 1928
[7] Köhler R, Tredicucci A, Beltram F, Beere H E, Linfield E H, Davies A G, Ritchie D A, Iotti R C and Rossi F 2002 *Nature* **417** 156
[8] Rochat M, Scalari G, Hofstetter D, Beck M, Faist J, Beere H E, Davies A G, Linfield E H and Ritchie D A 2002 *Electron. Lett.* **38** 1675
[9] Barbieri S, Alton J, Dhillon S S, Beere H E, Evans M, Linfield E H, Davies A G, Ritchie D A, Köhler R, Tredicucci A and Beltram F 2003 *IEEE J. Quantum Electron.* **39** 586
[10] Köhler R, Tredicucci A, Beltram F, Beere H E, Linfield E H, Davies A G, Ritchie D A, Dhillon S and Sirtori C 2003 *Appl. Phys. Lett.* **82** 1518
[11] Köhler R, Tredicucci A, Beltram F, Beere H E, Linfield E H, Davies A G and Ritchie D A 2003 *Opt. Lett.* **28** 810
[12] Scalari G, Ajili L, Faist J, Beere H E, Linfield E H, Ritchie D A and Davies A G 2003 *Appl. Phys. Lett.* **82** 3165
[13] Köhler R, Tredicucci A, Beltram F, Beere H E, Linfield E H, Ritchie D A and Davies A G 2003 *Electron. Lett.* **39** 1254
[14] Williams B S, Kumar S, Callebaut H, Hu Q and Reno J L 2003 *Appl. Phys. Lett.* **83** 2124
[15] Williams B S, Kumar S, Callebaut H, Hu Q and Reno J L 2003 *Appl. Phys. Lett.* **83** 5142
[16] Larrabee D C, Khodaparast G A, Tittel F K, Kono J, Scalari G, Ajili L, Faist J, Beere H E, Davies A G, Linfield E H, Ritchie D A, Nakajima Y, Nakai M, Sasa S, Inoue M, Chung S and Santos M B 2004 *Opt. Lett.* **29** 122
[17] Tredicucci A, Capasso F, Gmachl C, Sivco D L, Hutchinson A L and Cho A Y 1998 *Appl. Phys. Lett.* **73** 2101
[18] Köhler R, Iotti R C, Tredicucci A and Rossi F 2001 *Appl. Phys. Lett.* **79** 3920
[19] Köhler R, Tredicucci A, Beltram F, Beere H E, Linfield E H, Davies A G and Ritchie D A 2002 *Appl. Phys. Lett.* **80** 1867
[20] Tredicucci A, Gmachl C, Capasso F, Hutchinson A L, Sivco D L and Cho A Y 2000 *Appl. Phys. Lett.* **76** 2164
[21] Colombelli R, Capasso F, Gmachl C, Hutchinson A L, Sivco D L, Tredicucci A, Wanke M C, Sergent A M and Cho A Y 2001 *Appl. Phys. Lett.* **78** 2620
[22] Sirtori C, Gmachl C, Capasso F, Faist J, Sivco D L, Hutchinson A L and Cho A Y 1998 *Opt. Lett.* **23** 1366
[23] Ashcroft N W and Mermin N D 1988 *Solid State Physics* (Philadelphia: Saunders College) p 27
[24] Faist J, Beck M, Aellen T and Gini E 2001 *Appl. Phys. Lett.* **78** 147
[25] Williams B S, Callebaut H, Kumar S, Hu Q and Reno J L 2003 *Appl. Phys. Lett.* **82** 1015
[26] Kumar S, Williams B S, Kohen S, Hu Q and Reno J L 2004 *Appl. Phys. Lett.* **84** 2494
[27] Köhler R, Tredicucci A, Beltram F, Beere H E, Linfield E H, Ritchie D A and Davies A G 2004 *Appl. Phys. Lett.* **84** 1266
[28] Barbieri S, private communication
[29] Faist J, private communication
[30] Hu Q, private communication
[31] Mahler L, Köhler R, Tredicucci A, Beltram F, Beere H E, Linfield E H, Ritchie D A and Davies A G 2004 *Appl. Phys. Lett.* in press

Figure captions

Figure 1. (a) Conduction band energy diagram and moduli squared of relevant wavefunctions of the first 4.4 THz QC laser under an electric field of 3.5 kV/cm. The layer thicknesses can be found in [7]. The optical transition occurs between the two states drawn in boldface. Carriers are injected from the ground state into the upper laser level via resonant tunneling. Fast extraction of carriers from the lower laser level is facilitated by the strong coupling with the injector miniband. (b) Calculated waveguide mode profile along the growth direction of the final device structure. The origin of the abscissa is at the top metal-semiconductor interface; the laser active core is indicated by the shaded area.

Figure 2. Light-current (L-I) characteristics of a device originating from a nominally identical sample re-growth of the first THz QC laser described in Fig. 1. They have been recorded in pulsed operation at a duty cycle of 0.5% with a He-cooled Si bolometer. The bolometer was calibrated against the pyroelectric radiometer in the cw set-up, whose collection efficiency is estimated at 33%. Data refer to a laser with uncoated facets. The inset shows a laser spectrum recorded at high injection current at a heat sink temperature of 5 K, and clearly shows the wide comb of Fabry-Perot modes.

Figure 3. (a) Portion of the conduction band structure of the interlaced cascade design under an average electric field of 5.4 kV/cm. The optical transition is between the two states drawn in bold face and has a dipole moment of 7.2 nm. The layer thicknesses can be found in [27]. The phonon emission is indicated by the dashed arrow. Minibands A and B are connecting the phonon to the photon and the photon to the phonon stage, respectively. (b) Light-current characteristics of a 4.72 mm long and 150 μm wide device, recorded in pulsed operation, using the same calibration of Fig. 2, at a duty cycle of 3.5 μ% at heat sink temperatures of 6, 30, 50 and 80 K, respectively. The maximum output power of 10 mW is reached at 30 K and still 4 mW are obtained at 80 K. The device stops operating at 95 K. Note the very weak temperature dependence of the slope efficiency.

Figure 4. Left panel: Fabry-Perot emission spectra of quantum cascade lasers operating near 2.4 THz and 4.8 THz. The latter frequency is relevant for the detection of atomic oxygen. Right-panel: continuous wave light-current characteristics (33 % estimated collection efficiency) of a quantum cascade laser operating near 2.5 THz, a frequency region of interest for ozone monitoring. In the inset a typical emission spectrum is displayed.

Figure 5. Pulsed emission spectra of four different distributed feedback lasers driven close to the maximum output power. The left panel lasers feature a 9.4 μm grating period, while the right panel contains data of lasers with 9.2 μm gratings. Black curves refer to complete DFB lasers as described in the text; the gray multi-mode spectra originate from devices with no annealed-metal grating. In the latter case the coupling is almost purely real and, while no single-mode emission is observed, a clear stop-band gap is opened in the Fabry-Perot spectrum.

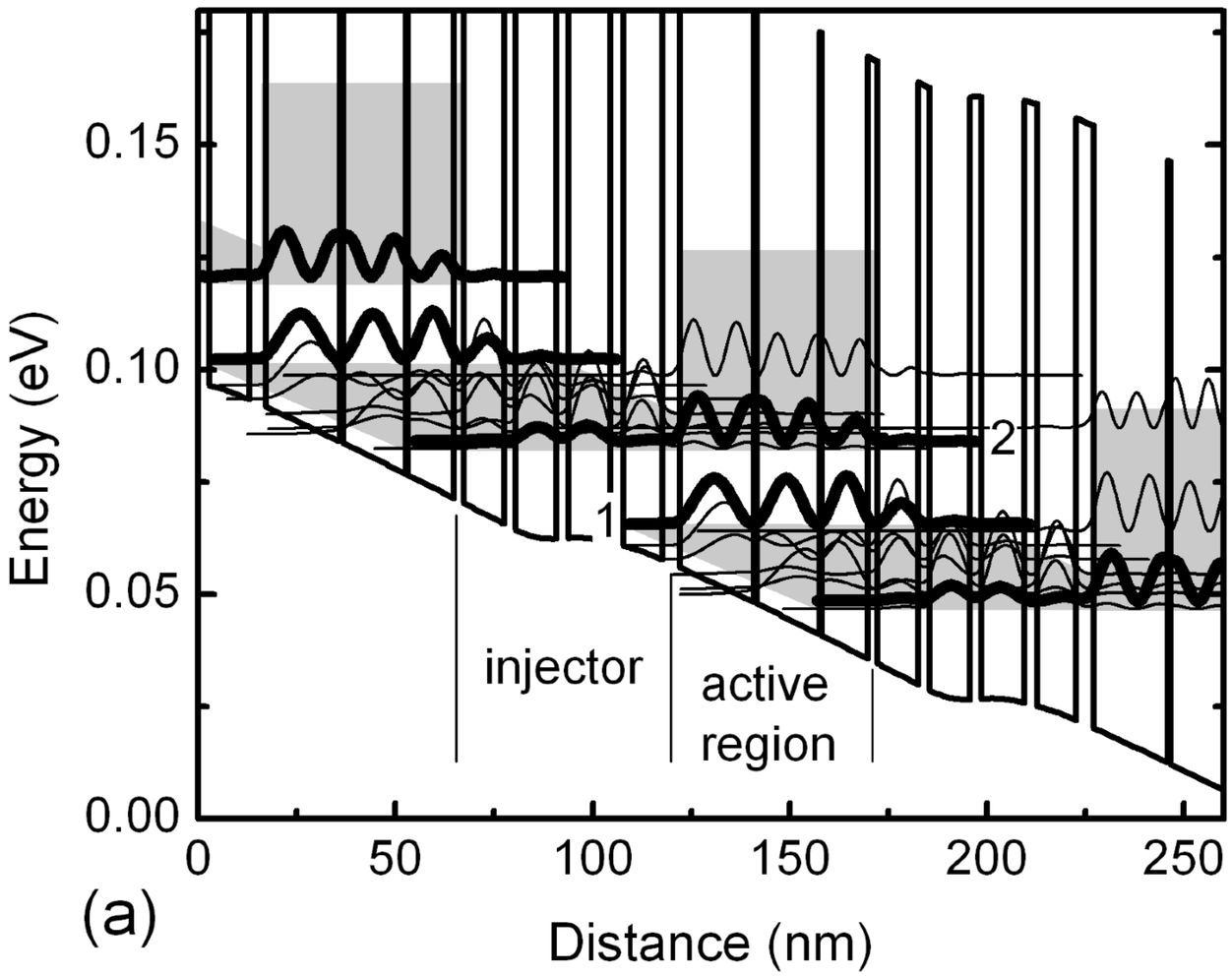
Energy (eV)
0.15
0.10
0.05
0.00
0
50
100
150
200
250
Distance (nm)
injector
active
region
1
2
(a)

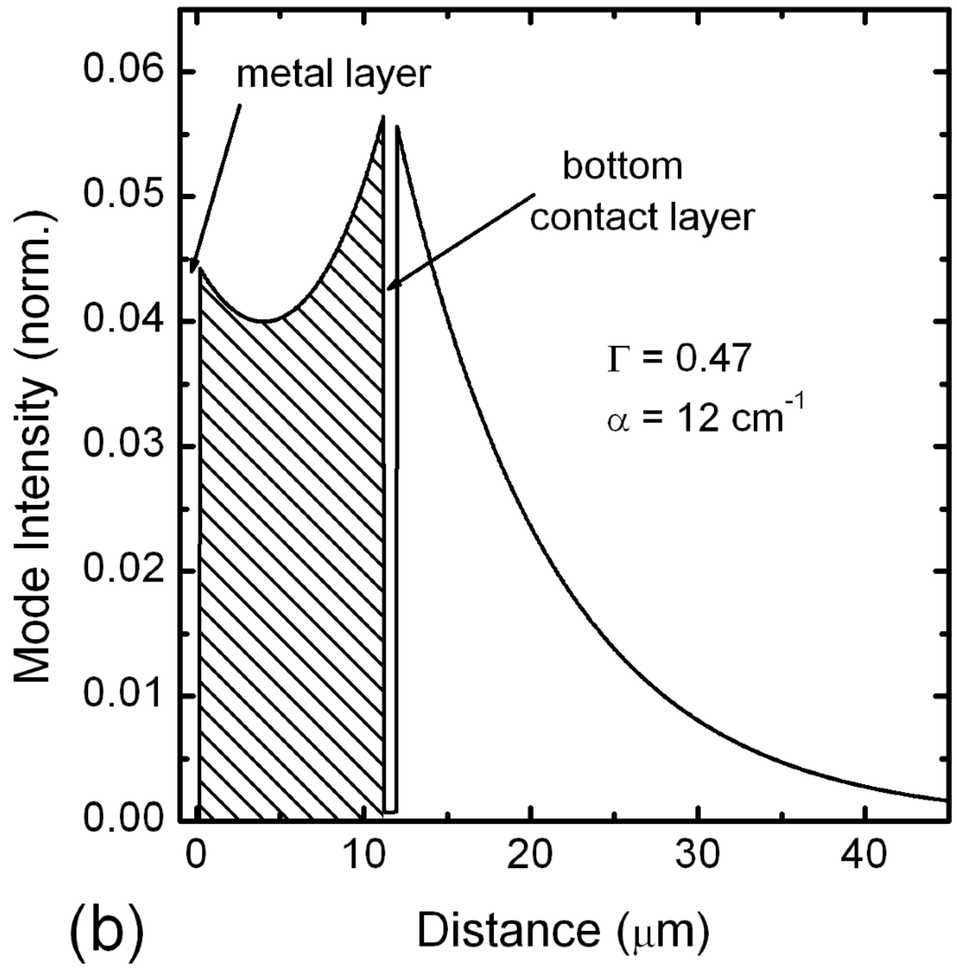
Mode Intensity (norm.)
0.06
0.05
0.04
0.03
0.02
0.01
0.00
0
10
20
30
40
Distance (μm)
metal layer
bottom
contact layer
Γ = 0.47
α = 12 cm-1
(b)

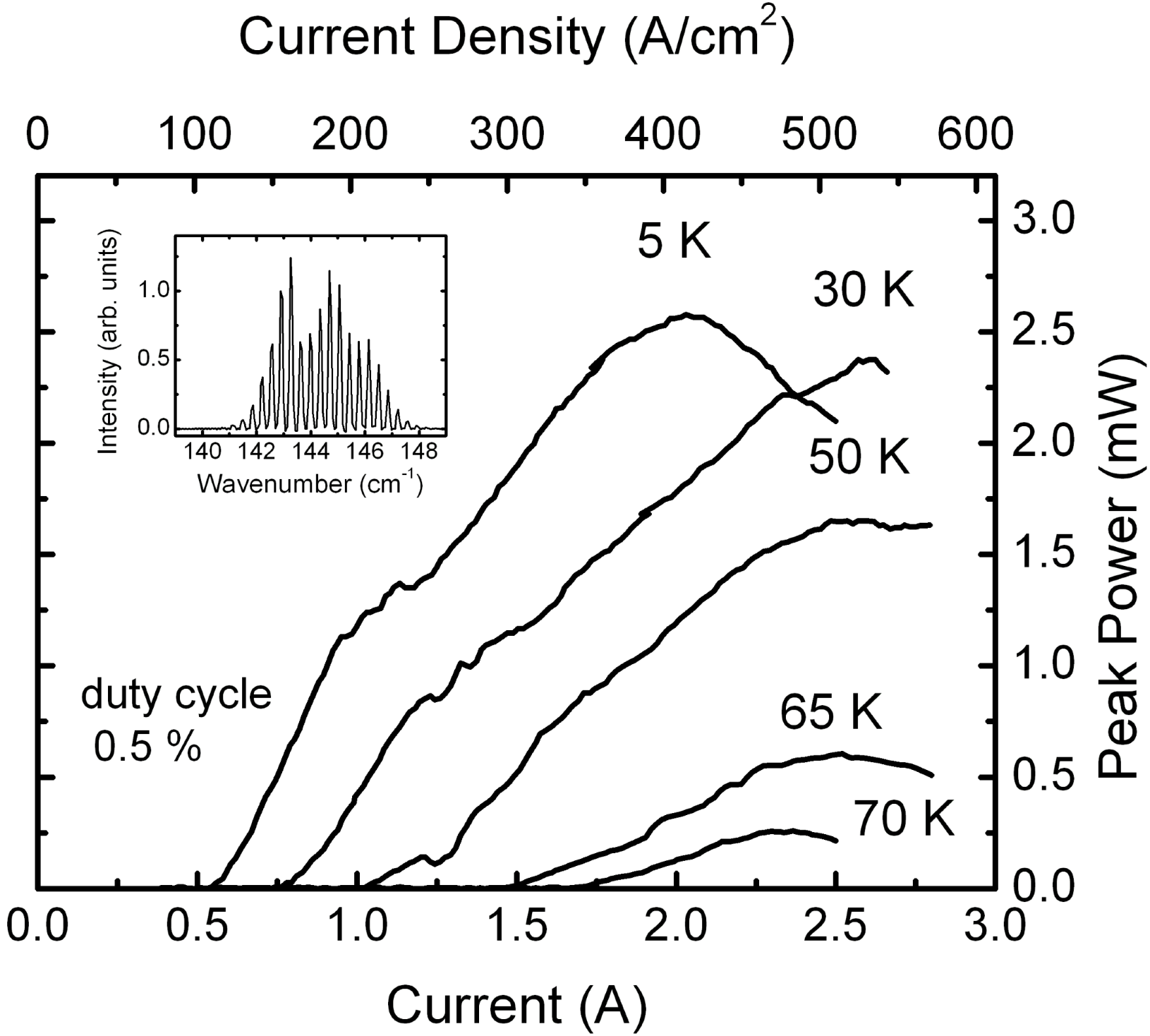
Current Density (A/cm^2)
0
100
200
300
400
500
600
5 K
30 K
50 K
65 K
70 K
duty cycle
0.5 %
Intensity (arb. units)
1.0
0.5
0.0
140
142
144
146
148
Wavenumber (cm^{-1})
3.0
2.5
2.0
1.5
1.0
0.5
0.0
Peak Power (mW)
0.0
0.5
1.0
1.5
2.0
2.5
3.0
Current (A)

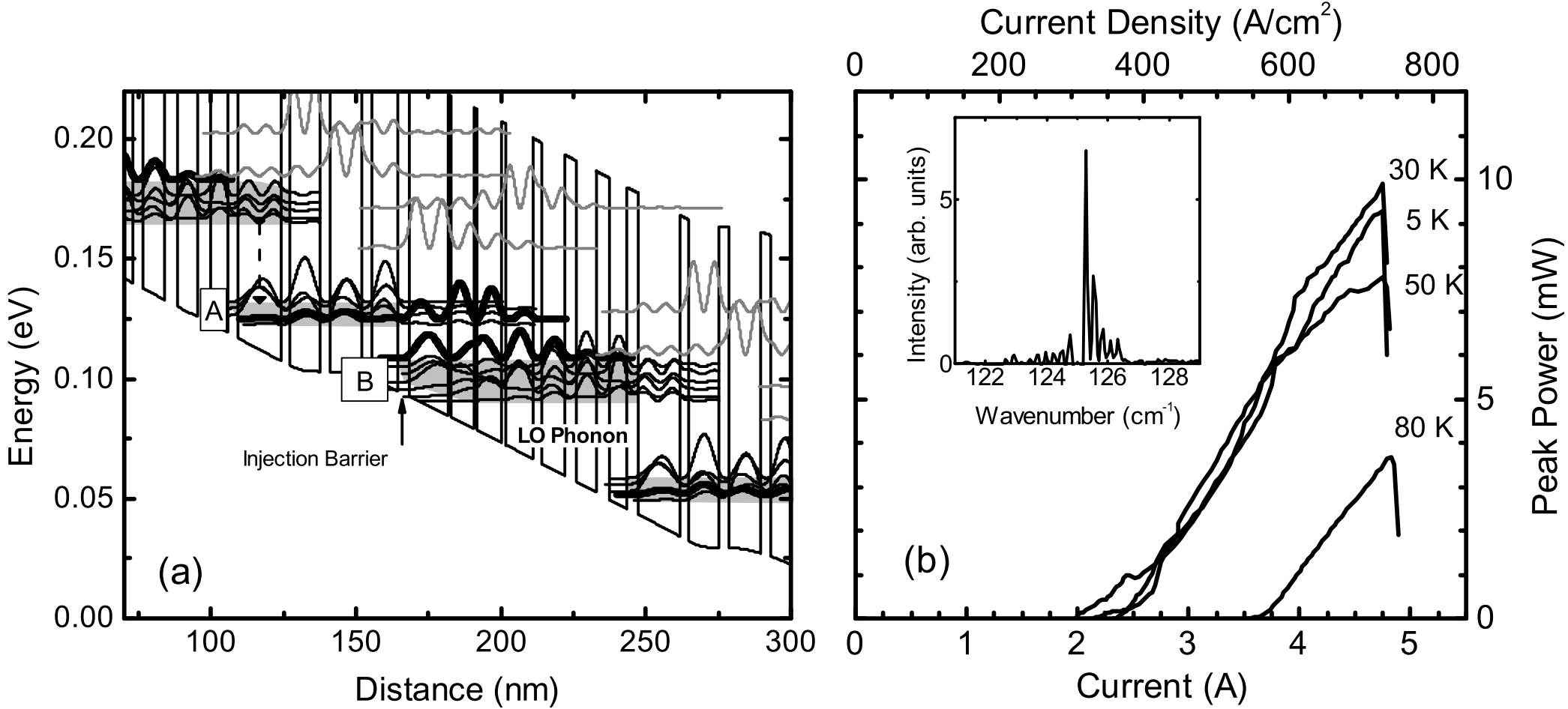
Energy (eV)
0.20
0.15
0.10
0.05
0.00
100
150
200
250
300
Distance (nm)
A
B
Injection Barrier
LO Phonon
(a)
Current Density (A/cm^2)
0
200
400
600
800
Intensity (arb. units)
5
0
122
124
126
128
Wavenumber (cm^{-1})
30 K
5 K
50 K
80 K
(b)
0
1
2
3
4
5
Current (A)
10
5
0
Peak Power (mW)

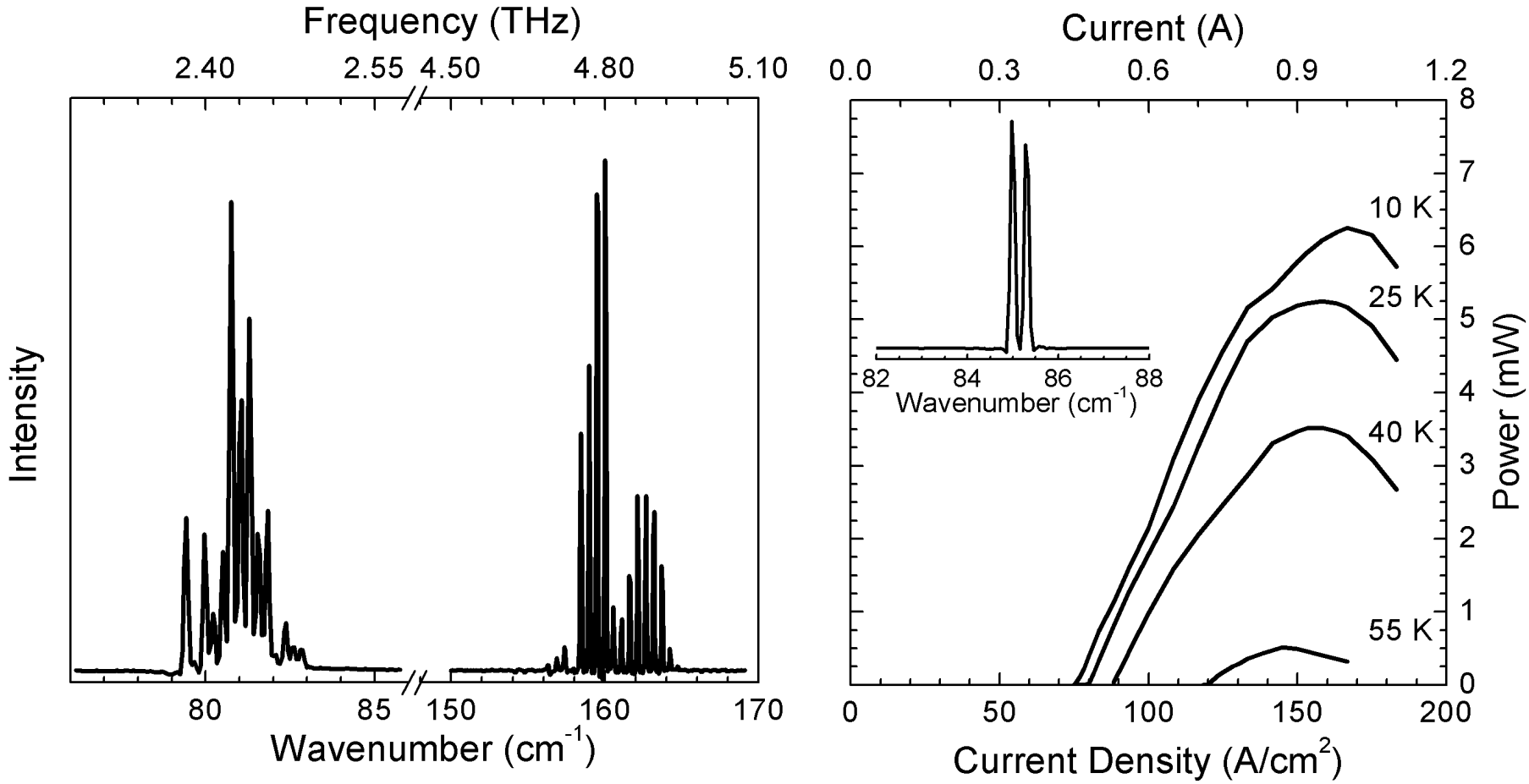
Frequency (THz)
2.40
2.55
4.50
4.80
5.10
Intensity
80
85
150
160
170
Wavenumber (cm-1)
Current (A)
0.0
0.3
0.6
0.9
1.2
82
84
86
88
Wavenumber (cm-1)
10 K
25 K
40 K
55 K
0
50
100
150
200
Current Density (A/cm2)
Power (mW)
0
1
2
3
4
5
6
7
8

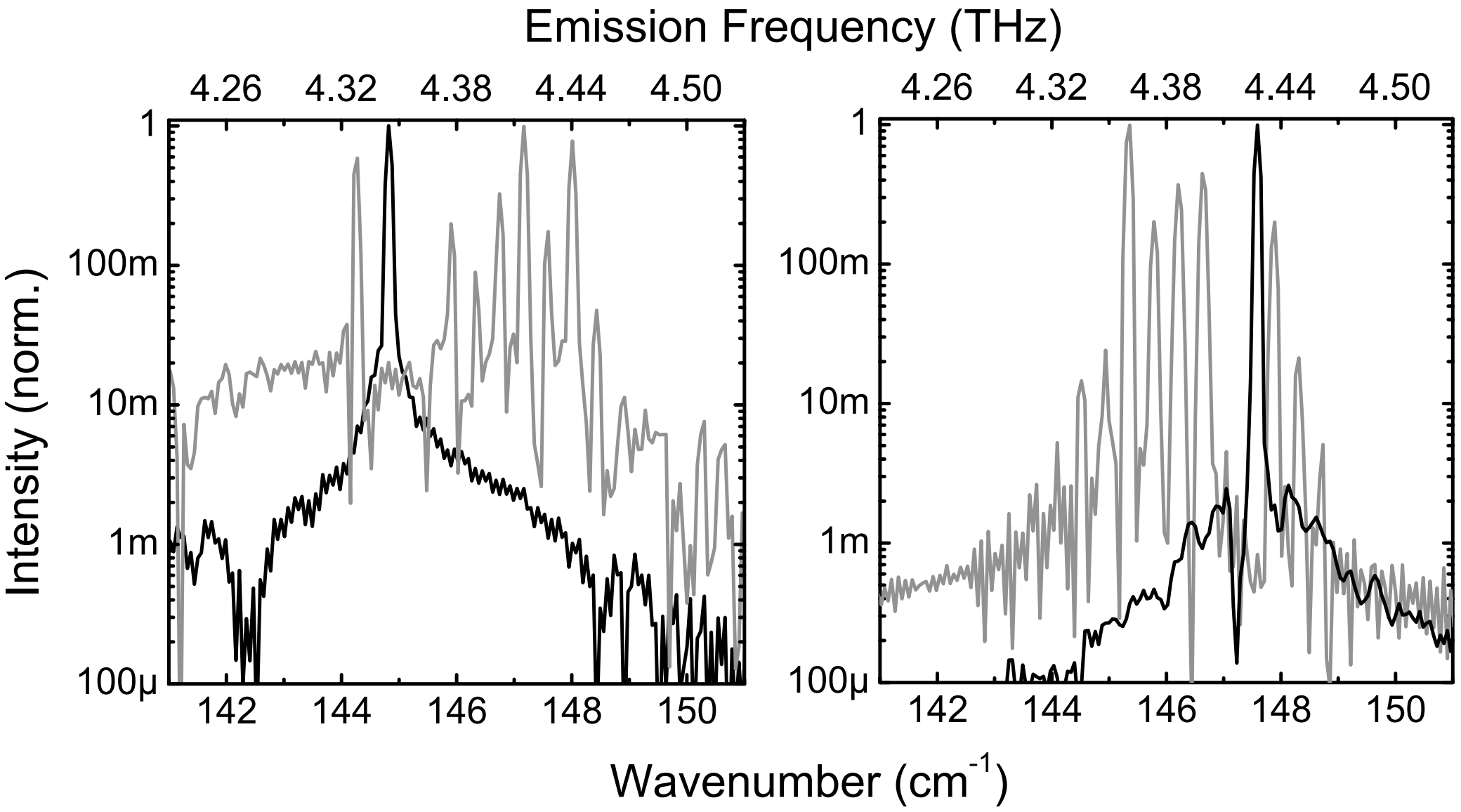
Emission Frequency (THz)
4.26
4.32
4.38
4.44
4.50
Intensity (norm.)
1
100m
10m
1m
100µ
142
144
146
148
150
Wavenumber (cm-1)